Research on Dynamic Response of Shell Structure under Underwater Shock Wave Load

Fantong Lin[a], Xianxiang Zhou[b], Lan Xiao[*], Chengfei Fan[c], Ziye Liu[d], Yifan Jia[e]

National Defense Engineering Research Institute, Academy of Military Sciences, Beijing, China

e-mail: [a]linfantong@126.com, [b]zhouxianxiang1@163.com, [c]tjufcf@163.com, [d]lzyy0011@163.com, [e]jiajocelyn@163.com
[*]Corresponding author's e-mail: festoon@sina.com

Abstract. To investigate the dynamic response of shell structure under underwater shock wave load, a three-dimensional numerical model for the typical shell structure under underwater shock wave load was established based on Arbitrary Lagrangian Eulerian algorithm. The dynamic response, deformation and failure mode of steel prefabricated hemispherical and semi-cylindrical sitting-bottom shell structures under different explosive equivalent and explosive distance were analyzed. The calculation results demonstrate that the peak displacement, deformation and effective stress increase with the increase of explosive equivalent and the decrease of explosive distance. The semi-cylindrical steel shell has obvious deformation in the mid-span area, the upper part of the bottom side constraints and the side walls at both ends. The upper part of the bottom constraints of the hemispherical steel shell deforms outward, but the overall deformation is small. When the explosive distance lower than 5m and the explosive equivalent lower than 200kg, the maximum effective stress of the hemispherical steel shell and the semi-cylindrical steel shell does not exceed the ultimate strength of Q690 steel.

Keywords: underwater shock wave load; shell; dynamic response; deformation mode; vertical displacement

1   Introduction

At present, there are many challenges in the development of underwater structures, such as the threat from underwater shock wave loads [1-2]. Underwater shock wave load has a short duration, but the intensity is extremely high. For example, the damage of the Nord Stream natural gas pipelines has aroused widespread attention from the world. A intense underwater shock wave load in the leak area of the Nord Stream gas pipeline was recorded at the measuring stations of Swedish and Danish. The integrity of the structure was affected by the excessive stress and strain caused by shock wave loads, leading to local failure and potential structural collapse [2]. Therefore, it is of great significance to evaluate the damage of underwater structure under underwater shock wave load.

In recent years, the impact of underwater shock wave load to important infrastructure has received extensive attention [2]. Therefore, it is need to consider the impact of underwater shock wave load to underwater structures. Some scholars have performed relevant research on the dynamic response of shell structures under underwater shock wave load. It mainly includes numerical simulation research on dynamic response of submerged tube tunnel under shock wave load [2], research on impact of surface shock wave load on tunnel dynamic response and anti-shock wave load performance [3], and research on damage assessment and mitigation measures of submerged tube tunnel under shock wave load [4]. The protective effects of covering layer thickness, carbon fiber reinforced polymer (CFRP) and ultra-high performance concrete (UHPC) on immersed tube tunnel under underwater shock wave load were verified. At present, there are few researches on the dynamic response of bottom-sitting shell structures under underwater shock wave load. Therefore, it is necessary to study the dynamic response of bottom-sitting shell structures under underwater shock wave load.

The multiple materials and shell structures are used in immersed tube tunnels and underwater pipelines. A normal working environment for the internal equipment and electronic components are provided by the pressure shell with sufficient strength and reliable sealing performance under underwater environment [5]. The prism or cylindrical shell is the main load-bearing structure of immersed tube tunnels and underwater pipelines mainly made of reinforced concrete or steel [6]. The stiffened cylindrical shell composed of pressure shell and reinforcement is the one of the main forms of submarine pressure structure [7]. In addition, the pressure spherical shell has attracted extensive attention due to its applications in underwater submersibles and civil engineering [8-9]. Therefore, considering the difficulty of underwater construction, the research on the dynamic response of semi-cylindrical or semi-spherical steel prefabricated shell structures under underwater shock wave load is carried out.

The damage of underwater structures under underwater shock wave load with high peak overpressure, slow attenuation and wide spread range are severer than onshore structures [10-11]. In addition to the threat of precision strikes, the fixed underwater shell structure is prone to be affected by far-field underwater shock wave load. Therefore, to further promote the construction of underwater shell structures and the development of related protection technologies, numerical simulation research on dynamic response of semi-cylindrical or semi-spherical steel prefabricated shell structures under far-field underwater shock wave load is performed, looking forward to provide scientific basis for the construction of underwater shell structures and the design of protective measures.

2   Finite Element Modeling

2.1   Material Models

TNT changes from a concentrated solid to a high-temperature and high-pressure gas with TNT is detonated. The relationship between product pressure, specific energy and volume during energy release is usually described by Jones-Wilkens-Lee (JWL) equation [12]:

$$P = A(1-\frac{\omega}{R_1 V})e^{-R_1 V} + B(1-\frac{\omega}{R_2 V})e^{-R_2 V} + \frac{\omega E_0}{V} \tag{1}$$

Where, P is the detonation product; A, B, ω are pressure coefficients; V is for specific volume; E_0 is the internal energy; R_1 is the principal eigenvalue; R_2 is a sub-eigenvalue; e is a constant. TNT parameters are shown in Table 1 [13].

Table 1. Parameters of JWL equation of state

ρ/km·m^{-3}	D/m·s^{-1}	P_{cj}/GPa	A/GPa	B/GPa	R_1	R_2	ω
1630	6930	21	373.77	3.747	4.15	0.9	0.35

The Gruneisen EOS equation of state is adopted in this research, and the pressure is defined as:

$$p = \begin{cases} \dfrac{\rho_0 C^2 \mu \left[1+(1-\frac{\gamma_0}{2})\mu - \frac{a}{2}\mu^2\right]}{\left[1-(S_1-1)\mu - S_2\frac{\mu^2}{\mu+1} - S_3\frac{\mu^3}{(\mu+1)^2}\right]} + (\gamma_0 + a\mu)E & \mu > 0 \\ \rho_0 C^2 \mu + (\gamma_0 + a\mu)E & \mu < 0 \end{cases} \tag{2}$$

Where, the specific volume $\mu = \rho/\rho_0 - 1$, ρ is the density of water and ρ_0 is the reference density; C is the intercept of particle velocity curve $v_s(v_p)$; S_1, S_2, and S_3 are dimensionless coefficients of the $v_s(v_p)$ slope; γ_0 is dimensionless Gruneisen gamma; a is a dimensionless first-order volume correction term. The parameters of Gruneisen EOS equation of state are shown in Table 2.

Table 2. Parameters of Gruneisen EOS equation of state

C/m·s^{-1}	S_1	S_2	S_3	a	γ_0	ρ /kg·m^{-3}
1647	1.921	-0.096	0	0	0.35	998.21

The LINEAR POLYNOMIAL EOS equation of state is adopted in this research, which is expressed as:

$$P = C_0 + C_1\mu + C_2\mu^2 + C_3\mu^3 + (C_4 + C_5\mu + C_6\mu^2)E_0 \tag{3}$$

Where, μ is defined as $\mu = \rho/\rho_0 - 1$, where ρ is the air density and ρ_0 is the reference density; the constants C_0-C_6 are the coefficients of EOS; E_0 is the initial specific internal volume of air. The material parameters of air are shown in the Table 3 [14].

Table 3. Parameters of LINEAR POLYNOMIAL EOS equation of state

ρ(kg/m^{-3})	C_0-C_3, C_6	C_4，C_5	E_0	V_0
1.25	0	0.4	2.53×10^5	1.0

The John-Cook model [15] is selected for the shell made of Q690 steel, and its expression is shown as:

$$\sigma = \left[A + B(\varepsilon^p)^n \right]\left(1 + C \bullet \ln \frac{\varepsilon'_p}{\varepsilon'_1}\right)(1 + T^{*m}) \qquad (4)$$

Where, A is the yield stress; B is strain hardening constant; C is the strain rate sensitive parameter; n is strain hardening index; ε^p and ε_p' are plastic strain and plastic strain rate, respectively; ε_1' is the reference strain rate; $T^{*m}=(T\text{-}T_r)(T_m\text{-}T_r)$, where m is the temperature softening index. The specific parameters are shown in the Table 4.

Table 4. John-Cook model parameters of Q690 steel

A/MPa	B/MPa	n	C	m
722	400	0.57	0.021	-

2.2   Finite Element Model Description

The fully coupled numerical model of bottom-sitting shell structure with underwater shock wave load is established using ALE numerical simulation method by commercial finite element software, as shown in Figure 1. The water area diameter is 8m, the length is 13m, and the shell structure dimensions are shown in Figure 2 and Figure 3 respectively. The steel shell is modeled by Lagrange method. The air, water and TNT are modeled by Euler method. The contact surface between the shell and water is modeled by fluid-structure coupling method, and the explosive is set by volume fraction form. The displacement of x, y and z direction at the bottom of the seated shell are set to zero.

(a) The coupling model of 1/4 hemisphere steel shell, water and shock wave

(b) The coupling model of 1/4 semi-cylindrical steel shell, water and shock wave

Fig. 1. The coupling model of 1/4 steel shell, water and shock wave
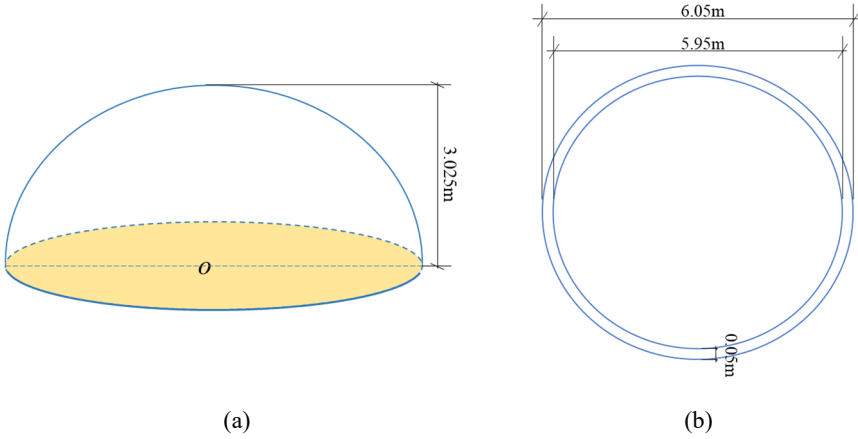
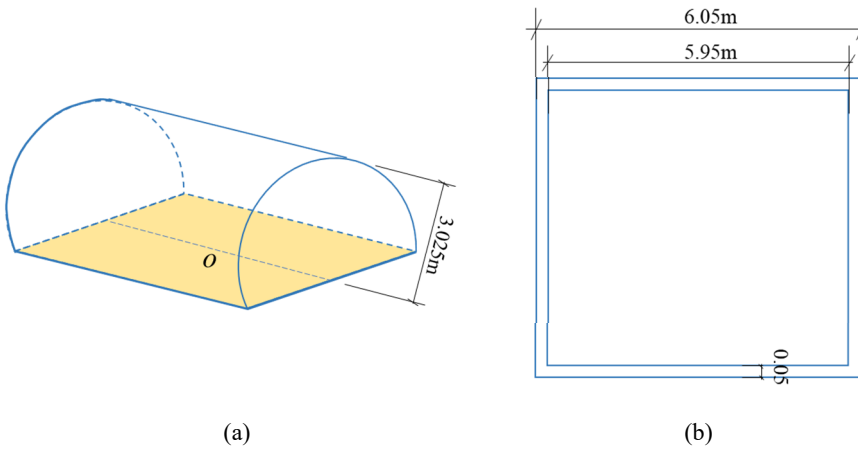Fig. 2. The dimensions of hemispherical sit-bottom steel shell

Fig. 3. The dimensions of semi-cylindrical sit-bottom steel shell

3   The Analysis and Discussion of Numerical Simulation Results

The explosive equivalent and explosive distance are main factors affecting the dynamic response of the structure. Therefore, the vertical displacement and deformation modes of semi-cylindrical and semi-spherical bottom-sitting steel shell under underwater shock wave load were studied by numerical model with the explosive distance that of 5m and 7m and explosive equivalent that of 25kg, 50kg, 100kg and 200kg respectively.

3.1 Influence of Explosive Equivalent and Explosive Distance on Vertical Displacement and Deformation Mode of Semi-Cylindrical Steel Shell

As shown in Figure 4 and Figure 5, at 0.01s, the relatively large values of the effective stress of the semi-cylindrical steel shell is located in the mid-span area of the shell, the junction between the semi-cylindrical shell and the side walls at both ends, and the position above the constraints on both sides of the semi-cylindrical shell. The effective stress of the steel shell increases with the increase of the charge and the decrease of the detonation distance. Meanwhile, when the explosive distance is 5m, the maximum effective stress of the semi-cylindrical steel shell is located in the mid-span area, and when the explosive distance is 7m, the maximum effective stress of the semi-cylindrical steel shell is located at the junction between the semi-cylindrical shell and the side walls at both ends.

At 0.01s, the upper constraints on both sides of the bottom of the semi-cylindrical shell are deformed outwards, and the deformation increases with the increase of explosive equivalent. When the explosive equivalent is 200kg, the maximum effective stress in the deformation area above the constraints on both sides of the bottom of the semi-cylindrical shell is about 387.9MPa with the explosive distance that of 5m, and the maximum effective stress in the deformation area above the constraints on both sides of the bottom of the semi-cylindrical shell is about 271.5MPa with the explosive distance that of 7m. Meanwhile, the inward deformation of both sides of the semi-cylindrical shell increases with the increase of the explosive equivalent. When the explosive equivalent is 200kg, the maximum effective stress at both ends of the semi-cylindrical shell is about 325.3MPa with the explosive distance that of 5m, and the maximum effective stress at both ends of the semi-cylindrical shell is about 227.7MPa with the explosive distance that of 7m. As shown in Figure 4, when the explosive equivalent is 200kg, the maximum effective stress in the mid-span area of the steel shell is about 638.3MPa, which does not exceed the ultimate strength of Q690 steel that of 770MPa.

The vertical deformation of the steel shell increases with the increase of the explosive equivalent, and the overall compression deformation occurs in the vertical direction. The center area of the shell has the largest vertical deformation. As shown in Figure 6, when the explosive distance is 5m, the vertical displacement of the center of the steel shell increases significantly with the increase of the explosive equivalent within 0.00254s-0.00865s, and when the explosive equivalent is 200kg, the peak vertical displacement of the center of the steel shell has a maximum value that of 0.0888m. As shown in Figure 7, when the detonation distance is 7m, the vertical displacement of the center of the steel shell increases significantly with the increase of the charge within 0.00370s-0.00960s, and when the explosive equivalent is 200kg, the peak vertical displacement of the center of the steel shell has a maximum value that of 0.0638m. When the explosive distance is 5m, the peak vertical displacement of the center of the steel shell is about 39.2% higher than 7m. In addition, some elastic recovery deformation occurs after the center of the semi-cylindrical steel shell reaches the first peak vertical displacement under the shock wave load.
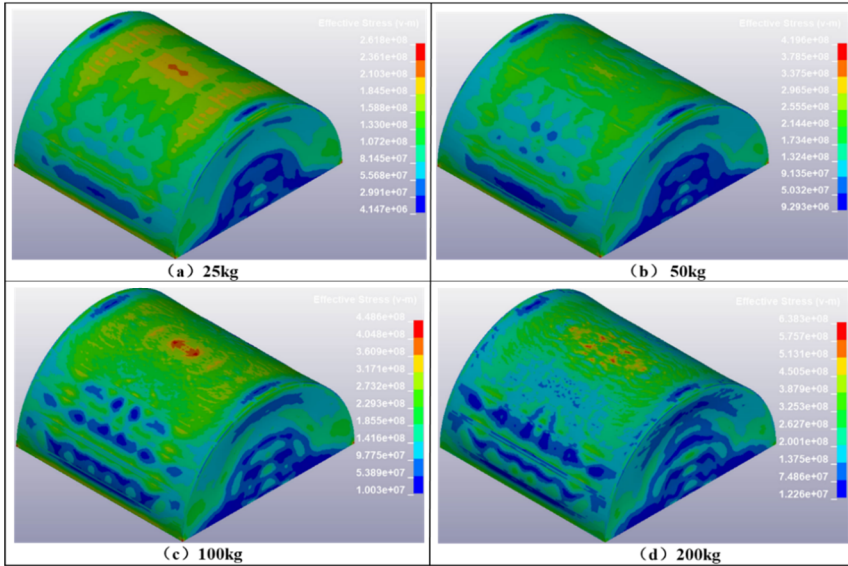
Fig. 4. Stress distribution diagrams of semi-cylindrical steel shell under different explosive equivalents with the explosive distance that of 5m
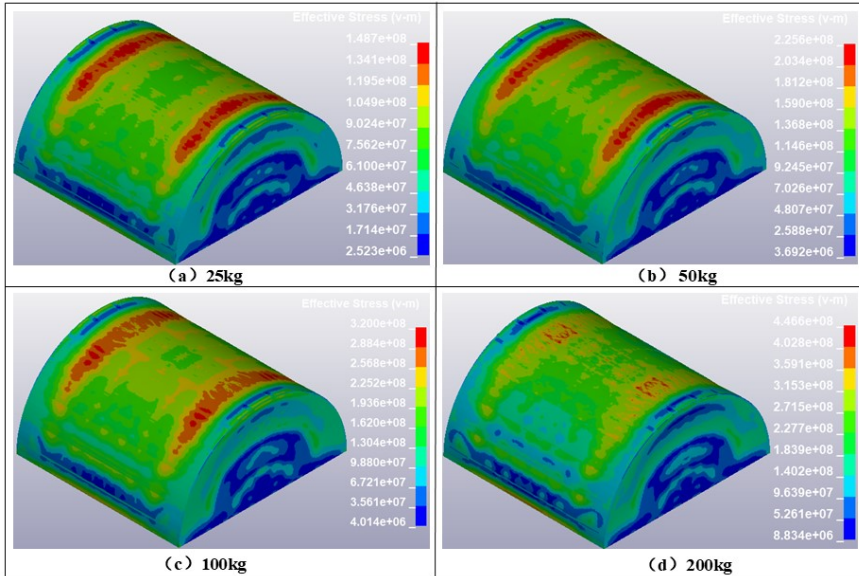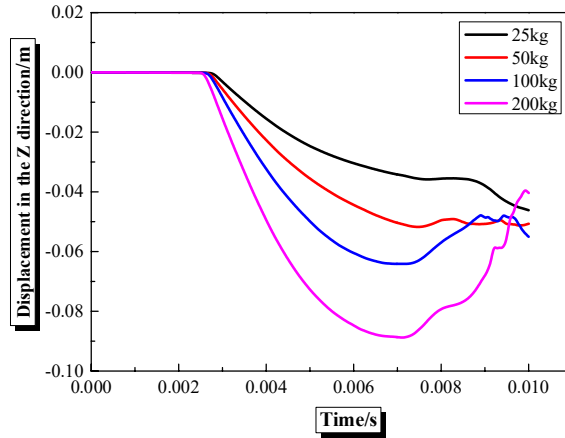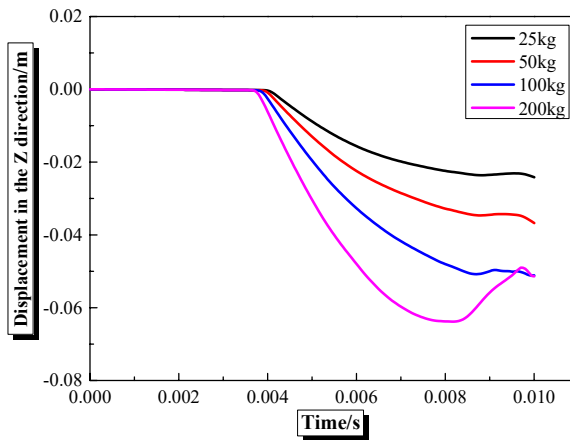

Fig. 5. Stress distribution diagrams of semi-cylindrical steel shell under different explosive equivalents with the explosive distance that of 7m

Fig. 6. Displacement time history of measuring points in vertical direction under different explosive equivalents with the explosive distance that of 5m
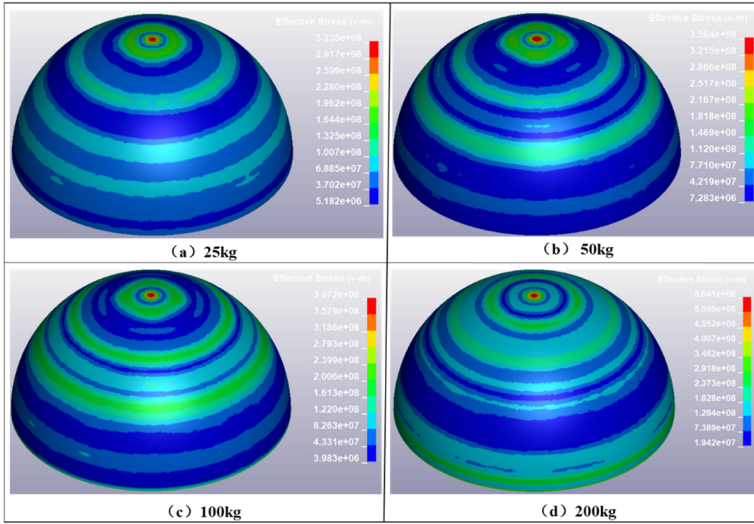

Fig. 7. Displacement time history of measuring points in vertical direction under different explosive equivalents with the explosive distance that of 7m

3.2 Influence of Explosive Equivalent and Explosive Distance on Vertical Displacement and Deformation Mode of Hemispherical Steel Shell

As shown in Figure 8, when the explosive distance is 5m, the maximum effective stress of the hemispherical steel shell is located in the center area of the shell at 0.01s. As shown in Figure 9, when the explosive distance is 7m, the maximum effective stress of the hemispherical steel shell presents a circular distribution at 0.01s, and gradually approaches the bottom of the shell with the increase of explosive equivalent. The effective stress of the steel shell increases with the increase of the charge and the decrease of the blast distance.

The upper position of the bottom constraint of the hemispherical steel shell deforms outwards at 0.01s, but the overall deformation of the hemispherical steel shell is small. When the explosive equivalent is 200kg, the maximum effective stress in the deformation area above the constraints on both sides of the hemispherical shell bottom is 346.2MPa at 5m explosive distance, and the maximum effective stress in the deformation area above the constraints on both sides of the hemispherical shell bottom is 220.9MPa at 7m explosive distance. As shown in Figure 8, when the explosive equivalent is 200kg, the maximum effective stress of the steel shell is 561.4MPa, which does not exceed the ultimate strength of Q690 steel that of 770MPa.

Fig. 8. Stress distribution diagrams of hemispherical steel shell under different explosive equivalents with the explosive distance that of 5m

The vertical displacement of the steel shell increases with the increase of the explosive equivalent. As shown in Figure 10, when the explosive distance is 5m, the vertical displacement of the center of the steel shell increases with the increase of the explosive equivalent within 0.00247s-0.00744s. When the explosive equivalent is 200kg, the peak vertical displacement is 0.0285m. As shown in Figure 11, when the explosive distance is 7m, the vertical displacement of the center of the steel shell increases with the increase of the charge within 0.00355s-0.00663s. When the explosive equivalent is 200kg, the peak vertical displacement is 0.0177m. When the hemispherical steel shell reaches the first peak vertical displacement, partial elastic recovery deformation occurs, and vertical oscillation deformation occurs later. When the explosive distance is 5m and the charge is 25kg, 50kg and 100kg, the vertical displacement oscillation of the center of the hemispherical steel shell is close with each other after the elastic recovery deformation. When the explosive equivalent is 200kg, the center position of the hemispherical steel shell still has a large vertical displacement after the elastic recovery deformation occurs. When the explosive distance is 7m, the center vertical displacement

and vertical oscillation are ultimately close with each other after the elastic recovery deformation of the hemispherical steel shell occurs.
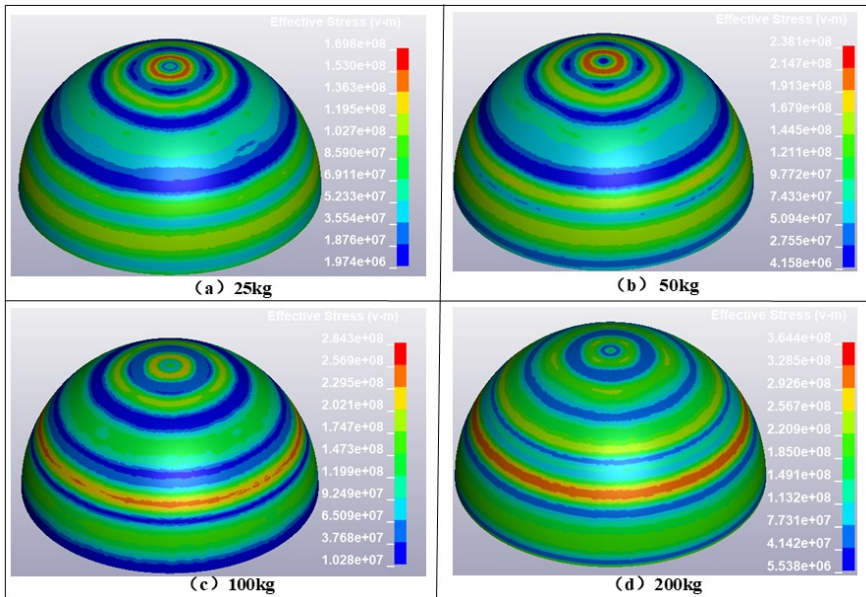

Fig. 9. Stress distribution diagrams of hemispherical steel shell under different explosive equivalents with the explosive distance that of 7m
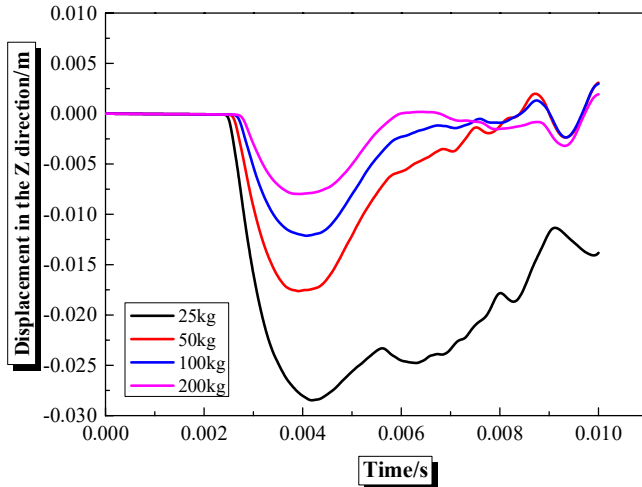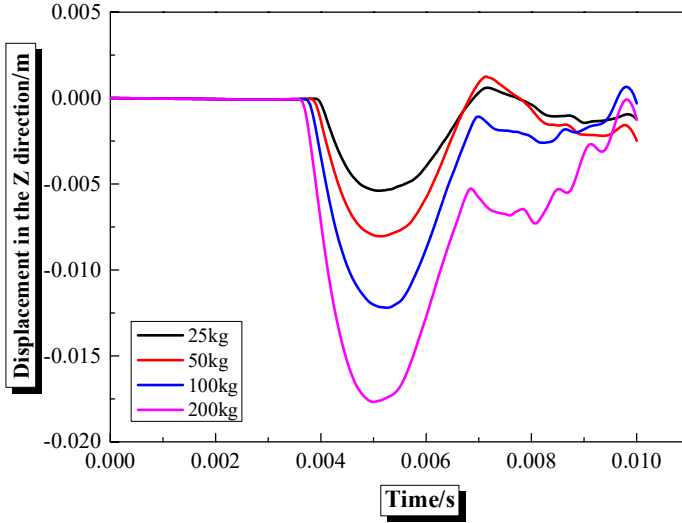

Fig. 10. Displacement time history of measuring points in vertical direction under different explosive equivalents with the explosive distance that of 5m

Fig. 11. Displacement time history of measuring points in vertical direction under different explosive equivalents with the explosive distance that of 7m

4   Conclusions

A coupled numerical model of bottom-sitting shell structure-water-shock wave was established to carry out numerical simulation research on dynamic response of prefabricated semi-cylindrical and semi-spherical bottom-sitting shell structures under underwater shock wave load. The main conclusions are as follows:

(1) The deformation and effective stress of the semi-cylindrical steel shell increase with the increase of explosive equivalent and the decrease of explosive distance. At 0.01s, the downward vertical deformation of the semi-cylindrical steel shell occurs in the mid-span region, outward deformation occurs in the upper position of the constraints on both sides of the bottom, and inward deformation occurs in the side walls at both ends. The larger effective stress of the semi-cylindrical steel shell is mainly located in the middle span area of the shell, the junction between the semi-cylindrical shell and the two sides of the side wall, and the position above the constraints on both sides of the semi-cylindrical shell.

(2) The deformation and effective stress of the hemispherical steel shell increase with the increase of explosive equivalent and the decrease of explosive distance. The overall deformation of the hemispherical steel shell is small under the given explosive distance and explosive equivalent. The upper position of the bottom constraint of the hemispherical shell was deformed outwards at 0.01s. When the explosive distance is 5m, the maximum effective stress is located in the center area of the outer surface of the shell. When the explosive distance is 7m, the maximum effective stress of the hemispherical steel shell presents a circular distribution, and gradually approaches the bottom of the shell with the increase of explosive equivalent.

(3) When the explosive distance lower than 5m and the explosive equivalent lower than 200kg, the maximum effective stress of the hemispherical steel shell and the semi-cylindrical steel shell does not exceed the ultimate strength of Q690 steel that of 770MPa.

References

1. Avachat S, Zhou M. Response of submerged metallic sandwich structures to underwater impulsive loads[J]. Journal of Mechanics of Materials and Structures, 2015, 10(1): 17-41.
2. Yang G D, Fan Y, Wang G H, et al. Numerical study on dynamic response of submerged tunnel subjected to underwater explosion[J]. Soil dynamics and earthquake engineering, 2022, 156: 107216.
3. Yang G D, Wang G H, Fan Y, et al. Dynamic response and performance of submarine tunnel subjected to surface explosions[J]. Marine Structures, 2021, 80: 103091.
4. Yang G D, Wang G H, Lu W B, et al. Numerical study on dynamic response of submerged tunnel subjected to underwater explosion subjected to blast loads[J]. Tunnelling and Underground Space Technology, 2019, 94: 103131.
5. Zhao Z W, Zhou S, Gao H, et al. Predictions of compression capacity of randomly corroded spherical shells based on artificial neural network[J]. Ocean Engineering, 2022, 257: 111668.
6. Guo J, Jiang S P, Zhang Z Y. Fire Thermal Stress and Its Damage to Subsea Immersed Tunnel[J]. Procedia Engineering, 2016, 166: 296-306.
7. MacKay J R, Jiang L, Glas A H. Accuracy of nonlinear finite element collapse predictions for submarine pressure hulls with and without artificial corrosion damage[J]. Marine Structures, 2011, 24: 292-317.
8. Zhang J, Lin Z K, Wang F, et al. Ultimate strength of externally pressurised steel spheres containing through-thickness defects[J]. International Journal of Pressure Vessels and Piping, 2022, 199: 10470.
9. Zhang J, Zhang M, Tang W X, et al. Buckling of spherical shells subjected to external pressure: A comparison of experimental and theoretical data[J]. Thin-Walled Structures, 2017, 111: 58-64.
10. Lu C F, Chen W Q, Shao J W. Semi-analytical three-dimensional elasticity solutions for generally laminated composite plates[J]. European Journal of Mechanics A/Solids, 2008, 27(5): 899-917.
11. Wang H M. Dynamic electromechanical behavior of a triple-layer piezoelectric composite cylinder with imperfect interfaces[J]. Applied Mathematical Modelling, 2011, 35(4): 1765-1781.
12. Lee E L, Hornig H C, Kury J W. Adiabatic expansion of high explosive detonation products. UCRL-50422, Lawrence Radiation Laboratory, University of California, 1968.
13. Yang G D, Fan Y, Wang G H, et al. Blast resistance of air-backed RC slab against underwater contact explosion[J]. Defence Technology, 2022.
14. Xie L X., Lu W B., Zhang Q B, et al. Analysis of damage mechanisms and optimization of cut blasting design under high in-situ stresses[J]. Tunnelling & Underground Space Technology, 2017, 66: 19-33.
15. Yang X, Yang H, Zhang S. Rate-dependent constitutive models of S690 high-strength structural steel[J]. Construction and Building Materials, 2019, 198: 597-607.